CHAPTER VII
SYNTHESIS OF Pd OR V DEPOSITED MWNTS AND THEIR HYDROGEN STORAGE CAPACITY

7.1 Abstract

This work presents synthesis and characterization of Pd or V deposited carbon nanotubes (CNTs) - multi-walled type (MWNTs) - including hydrogen storage capacity measured by using Sievert's volumetric apparatus. CNTs were grown by the CVD method using LPG and $LaNi_5$ as a carbon source and catalyst, respectively. Pd was impregnated on the CNTs by the reflux method using hydrogen gas as a reducing agent while V was embedded on the CNTs by the vapor deposition method. The average metal particle size deposited on the CNTs was around 5.8 nm or 3.6 nm for Pd and V, respectively. Hydrogen sorption experiments were performed at room temperature and at -196°C under hydrogen pressure of 65 bar. It was found that at -196°C, the purified CNTs had the maximum hydrogen uptake of 1.21 wt% while the Pd-CNTs and V-CNTs possess lower surface areas inducing lower hydrogen adsorption capacity of 0.37 wt% and 0.4 wt%, respectively. For the hydrogen sorption at room temperature, the CNTs decorated with metal nanoparticles had a higher hydrogen uptake compared to the purified CNTs. Hydrogen sorption capacity was 0.125 wt% and 0.1 wt% for the Pd-CNTs and V-CNTs, respectively, while the hydrogen uptake of the purified CNTs was < 0.01 wt%. For the second cycle, only half of the first hydrogen uptake was obtained, and this was attributed to the re-crystallization of defect sites on the carbon substrate after the first hydrogen desorption.

Keywords: CNTs, Hydrogen storage, Adsorption, Absorption

7.2 Introduction

In recent years, carbon nanotubes (CNTs) have been shown to be one of the most promising materials for nanotechnology based applications such as catalysis, nanocomposites, micro- and nano-electronic devices, electrodes, and batteries [1]. In

addition, it has been suggested that CNTs can be a promising medium for on-board hydrogen storage with high surface area and hollow space inside, which could provide the needed capacity for hydrogen storage [2]. However, early experimental data on hydrogen storage using CNTs contradicted theoretical calculations, and there have been a large variation in the CNT hydrogen storage capacity reported by various research groups. For example, hydrogen adsorption characteristics of single walled carbon nanotubes (SWNTs) were investigated, and the hydrogen capacity was found to be in the range of 0.01-10 wt% [3-4]. In contrast, multi-walled carbon nanotubes (MWNTs) were reported to have a hydrogen uptake of up to 14 wt% at room temperature and ambient pressure when doped with an alkaline metal [5]. In a later work by Yang *et al.* [6], it was determined that the high hydrogen capacity of the alkaline metal-doped MWNTs was actually caused by moisture in the hydrogen gas, and that the alkaline-doped MWNTs could only adsorb ~ 2 wt% hydrogen. Different hydrogen storage capacity, using CNTs was reported to depend upon preparation methods, conditions in experiments, purity of CNTs, adsorption conditions, and errors from the measurements [7]. However, in practice, a small amount of hydrogen can be stored by pristine CNTs. Many research groups have attempted to improve the hydrogen sorption capacity of CNTs by modification of the relatively inert surface, which could be the cause of the difficulties encountered for hydrogen sorption [3, 8]. Using CNTs decorated by metal nanoparticles, such as Pt and Pd, seems to be a promising method to improve hydrogen adsorption onto CNTs. Such metals are known to play a role in the dissociation of hydrogen, followed by atomic hydrogen spillover and finally absorption onto the support [9-11]. Recently, Yildirim and Ciraci [12] reported a first-principle computational study on the interaction between hydrogen molecules and Ti or V atoms adsorbed on SWNTs. They found that a single Ti atom adsorbed on SWNTs can strongly bind up to four hydrogen molecules. In other words, SWNTs decorated with Ti can strongly adsorb up to 8 wt% hydrogen. However, this data is still from a theoretical point of view. In this work, we report the hydrogen sorption capacity of treated MWNTs compared with CNTs decorated with Pd or V.

7.3 Experimental

7.3.1 CNT synthesis and treatment

CNTs were synthesized using chemical vapor deposition method (CVD). Liquid petroleum gas (LPG, Afrox South Africa) was used as a carbon source and $LaNi_5$ (Guangzhou Research Institute for Non-Ferrous Metals, China) used as a catalyst. $LaNi_5$ was treated before using in the experiment by stirring with 0.2 M HCl for 30 min then filtered and washed with deionized water. About 2 g of treated $LaNi_5$ powder was loaded into a quartz combustion boat and placed inside a quartz tube located inside a tube furnace. The system was sealed and flushed with nitrogen for 10 min, and then the temperature was ramped to 800°C. Once the temperature was stabilized, the nitrogen flow was cut off and LPG flow was initiated at a flow rate of 5.8 cm^3 min^{-1}. After 60 min, the LPG flow was terminated and the nitrogen flow was re-initiated. The sample was then cooled under nitrogen. The schematic of apparatus is shown in Figure 7.1.

After CNTs synthesis, the raw CNTs were purified by acid solution. 2 g of CNTs were added to 100 ml of 10 M HCl. The mixture was sonicated (ultrasonic bath, integral systems, model UMC-20, 50 kHz, 400 watts) for 1 h and refluxed at 120°C for 3 h. The solid was filtered and washed with deionized water until pH value of the rinsed water was around 6-7, and dried in an oven at 90°C overnight. Before metal deposition, the purified CNTs were modified through oxidation by concentrated HNO_3 under ultrasonication for 1 h.

7.3.2 Metal deposition on CNTs

Metal deposition on CNTs was prepared by two methods. The first method was the reflux method for Pd deposition. 0.001 M $PdC_{10}H_{11}O_4$ (98%, Aldrich Chemical) in toluene was added in 0.5 g purified CNTs. The mixture solution was stirred and sonicated for 30 min, and then 10% H_2 gas balanced with Argon (99.9995%, Afrox South Africa) was bubbled through the former mixture under the reflux condition at 130°C. The filtered solid was washed with toluene and dried in a vacuum oven at 120°C overnight. For V deposition, 0.5 g purified CNTs were mixed with $VC_{15}H_{21}O_6$ (98%, Aldrich Chemical) using mortar. The powder was loaded in a

reactor, vacuumed and heated to 450°C for 1 h. The amount of deposited metal on CNTs was approximately 10%. The samples were characterized by a scanning electron microscope and EDS detector (SEM, Leo F440), transmission electron microscopy (TEM, Hitachi 600), thermogravimetric analysis (TGA, Rheometric Scientific STA 1500 TGA/DSC, room temperature to 850°C, air flow rate of 14.5 cm^3 min^{-1}, heating rate of 5°C min^{-1}), X-ray diffractometer (Rigaku, Cu-Kα radiation, 40 kV, 30 mA), FT-Raman spectroscopy (Perkin Elmer, Spectrum GX, 40 mW, Resolution of 16 cm^{-1}), nitrogen adsorption/desorption at 77K (Micrometrics Tristar Surface analyzer) with Brunauer-Emmet-Teller (BET) analysis, and inductively coupled plasma spectrometry (ICP, Optima 4300DV, Perkin Elmer Instrument).

7.3.3 Hydrogen storage capacity

Hydrogen sorption on samples were measured by Sievert's apparatus, as shown schematically in Figure 7.2, equipped with a vacuum pump, vacuum gauge, three pressure transducers in different pressure range (0.3% accuracy, Gem Sensors), digital read out and record set (34970A data acquisition and switch unit, Agilent). All reactors, valves, and fittings were purchased from Swagelok. Some parts of the apparatus were put into a temperature controlled unit in order to prevent errors due to the change in the ambient temperature. Approximately, 900 mg of a sample were used for each measurement. Before starting the hydrogen sorption experiment, the degassing procedure was conducted at vacuum condition ~ 10^{-2} mbar, from room temperature to 400°C for 1 h to remove remaining gases. Subsequently, hydrogen (purity >99.999%) was fed into the sample holder at 400°C and hydrogen pressure of ~ 65 bar. The system was held under this condition until the pressure was stable in order to activate the sample. Then, the system was cooled down to room temperature. Hydrogen sorption was operated at the liquid nitrogen temperature (-196°C) and room temperature (20°C) with an initial hydrogen pressure ~ 65 bar. After the hydrogen sorption, hydrogen gas was released from the system by heating up to 380°C. The same procedure was repeated to investigate the reversibility. Hydrogen sorption data obtained were calculated as mass of adsorbed hydrogen/mass of

adsorbent materials (weight percent). All the calculations were carried out using real gas law with precise calculations of H_2 compressibility factor, Z(P,T), similar to the one described elsewhere [13]. The correction of internal reactor volume (by subtracting sample volume) was done starting from the estimated sample density of ~ 1.4 g cm^{-3}.

7.4 Results and discussion

Figure 7.3 shows the typical TEM images of MWNTs obtained using $LaNi_5$ as a catalyst (Figure 7.3(a)) and after treatment with acid solution (Figure 7.3(b)). Clean surface and hollow center of the CNTs can be clearly observed. The diameter sizes of MWNTs are below 100 nm. After the purification with HCl, the CNTs were treated with HNO_3 using ultrasound in order to create defect sites on their surfaces. The stability and impurity of the CNTs were characterized by TGA as shown in Figure 7.4. The raw CNTs and purified CNTs begin to be oxidized at 480 - 630°C while the oxidation temperature of the CNTs treated by HNO_3 is lower in the range of 200 - 630°C. This shows that the CNTs are oxidized by HNO_3 during the sonication, creating defect sites or functional groups on the surface of the CNTs leading to lower oxidation temperature. TGA analyses further show that the metal trace is about 4 wt% in the CNTs after the HCl purification and only about 2 wt% after further treatment with HNO_3.

TEM images presented in Figure 7.5 indicate the high dispersion of Pd nanoparticles supported on the CNTs (Pd-CNTs). The metal particle size was determined from the TEM images by measuring more than 100 particles. The Pd particle sizes are between 3 - 25 nm while the average particle size is 5.8 nm. However, we can observe the bulk of Pd due to the agglomeration of Pd particles. Figure 7.6 shows the TEM images of V nanoparticles supported on the CNTs (V-CNTs). The uniformity of particle distribution on the surface of the CNTs is evidenced. The mean particle size for V supported on the CNTs is 3.6 nm. The XRD patterns of the samples are displayed in Figure 7.7. The XRD data show that the CNTs still exhibit a good ordered structure after the acid purification and treatment,

as evidenced by the (002) and (100) peaks (Figures 7.7(a) and (b)), which are defined as the reflections of hexagonal graphite [14-15]. The XRD pattern of Pd supported on the CNTs is in the form of Pd^0 (Figure 7.7(c)) while the V peak cannot be observed in Figure 7.7(d). This implies that the size of V may be too small to be detected by the XRD technique. The actual amount of metal deposited on the CNTs was identified by the ICP technique. As a result, the amount of Pd deposited on the CNT is 7.91 % , which is more than that of V, 5.81 %. However, the exact amounts of the metal deposited on the CNTs are lower than the expected amount. In the case of vapor deposition, some V may have deposited on the wall of the container, not just only on the CNTs.

The hydrogen sorption capacity of all samples is shown in Table 7.1. At the sorption temperature of -196°C, the amount of adsorbed hydrogen on the samples seems to be related to the surface area of the absorbents as the main sorption mechanism is physisorption. As the result, the purified CNTs with the highest surface area have the highest hydrogen uptake, 1.2 wt%, while Pd-CNTs and V-CNTs possess lower surface areas inducing lower hydrogen sorption capacity. The purified CNTs have open ends due to the action of the acids treatment oxidizing and removing any caps, either in the form of metal nanoparticles and/or carbon layers, on the CNTs (see Figure 7.4). Once the metal (V or Pd) is deposited onto the purified CNTs, these same openings are once again blocked by the nanoparticles. As the result, the specific surface area for the functionalized CNTs decreases, despite the increase in the dispersion of the nanoparticles. Similar trends have been observed by Zhao *et al.* [16] with Pt deposited on CNTs and activated carbon. This may be explained that some metals deposited on CNTs may block the N_2 adsorption, and cause the decrease in the BET surface area of the doped samples. The hydrogen sorption at room temperature is lower than 0.01 wt% for the CNTs, and 0.1 and 0.125 wt% for the V-CNTs and Pd-CNTs, respectively. This could be explained that as the temperature is higher, the catalytic activity of metal enhances the hydrogen dissociation. After the dissociation, the dissociative hydrogen chemisorbs on the metal sites or diffuses to adsorb/absorb at defect sites of carbon substrates.

As the normalization of hydrogen uptake on a metal basis shows that the H:Pd ratio of Pd-CNT is 1.67, which is higher than the hydrogen uptake of only Pd

bulk, ~ 0.8 H/Pd at 60 bar and 20°C [17-18]. Thus, this result indicates that there are some hydrogen atoms absorbed on the CNTs. In the case of V-CNTs, the H:V ratio is 0.96 while the maximum hydrogen uptake of V metal is up to 1.9 H/V [19]. The hydrogen uptake of V-CNTs would result from the hydrogen absorption in V to form vanadium hydride. The reason why the hydrogen uptake of V does not reach the maximum capacity is because V is not fully hydrogenated in the form of VH_2 (γ phase) but rather in the form of V_2H (β_1 phase) or VH (β_2 phase) instead. Due to the instability of the γ phase of vanadium hydride, it can absorb and release hydrogen at moderate temperature and pressure. Consequently, this results in only half of the amount of hydrogen absorbed in the V metal, which was reported by Reilly *et al.* [20 -21].

In the second hydrogen sorption, hydrogen uptake of V-CNTs is about 0.08 wt% (0.764 H/V), nearly the same as the value of the first cycle. This result supports that the hydrogen sorption of V-CNTs mainly takes place on V and hydrogen would not migrate to the carbon support. In the case of Pd-CNTs, the hydrogen uptake decreases by half of the first hydrogen sorption, 0.065 wt% (0.866 H/Pd). We believe that the lower hydrogen capacity of the sample in the second cycle is because of the re-crystallization of defect sites after the hydrogen desorption at high temperature. This leads to a lack of defect sites to accept any dissociative hydrogen from Pd. In addition, the re-crystallization of the defect sites causes the decrease in the interaction between the metal and carbon support, which is an important factor for hydrogen migration to the support. This hypothesis is further confirmed by the ratio value of the D-band and G-band from the FT-Raman spectroscopy as shown in Figure 7.8. The D/G ratio, which indicates the degree of disorder structure of CNTs, decreases after the hydrogen absorption/desorption [22]. From the results, Pd contributes in the dissociation of hydrogen but its evidence on the hydrogen spillover cannot be clearly observed. An increase in the interaction between the metal and carbon support and stability of defect sites on the carbon surface would contribute the dissociative hydrogen to migrate to carbon support.

7.5 Conclusions

CNTs were grown by the CVD method using LPG as the carbon source and $LaNi_5$ as the catalyst. Pd deposited on the CNTs was obtained by using the reflux method with hydrogen bubbling while the vapor deposition method was used to embed V on the CNTs. The average Pd particle size deposited on the CNTs was around 5.8 nm and that of V was 3.6 nm. The hydrogen uptake of the samples was measured using Seivert-type apparatus. At -196°C, the purified CNTs showed the maximum hydrogen uptake of 1.21 wt% while the Pd-CNTs or V-CNTs had the hydrogen uptake of 0.37 wt% and 0.4 wt%, respectively. This is because the purified CNTs had the highest specific surface areas compared with those of the Pd-CNTs or V-CNTs. This indicated that physisorption was the mechanism responsible for hydrogen uptake, which correlates with the surface area. For the hydrogen sorption at room temperature, the CNTs deposited with one of the metals showed hydrogen uptake higher than the purified CNTs. Hydrogen sorption capacity was 0.125 wt% and 0.1 wt% for Pd-CNTs and V-CNTs, respectively. For the second cycle, only half of the first hydrogen uptake can be obtained. This is because the lack of defect sites to accept any dissociative hydrogen from Pd due to the re-crystallization of the defect sites on the carbon substrate after the hydrogen desorption at high temperature. Moreover the re-crystallization of the defect sites also leads to the decrease in the interaction between metal and carbon support. And this prevents the dissociative hydrogen to migrate to the carbon surface. Thus, the main hydrogen uptake of Pd-CNTs or V-CNTs in the second cycle resulted from the hydrogen absorption of the metal in the form of metal hydride.

7.6 Acknowledgment

This work was supported by South African Institute for Advanced Materials Chemistry (SAIAMC), University of the Western Cape, The Petroleum and Petrochemical College (PPC), Chulalongkorn University, National Science and Technology Development Agency (Reverse Brain Drain Project), and UOP LLC. We

would also like to thank Department of Physics, University of the Western Cape for assistance with the TEM work.

7.7 References

[1] Ang LM, Hor TSA, Xu GQ, Tung CH, Zhao SP, Wang JLS. Decoration of activated carbon nanotubes with copper and nickel. Carbon 2000;38:363-372.

[2] Dillon AC, Heben MJ. Hydrogen storage using carbon adsorbents: past, present and future. Appl Phys A Mater Sci Process 2001;72:133-142.

[3] Hirscher M, Becher M, Haluska M, Zeppelin FV, Chen X, Weglikowska UD, Roth S. Are carbon nanostructures an efficient hydrogen storage medium?. J Alloys and Compds 2003;356-357:433-437.

[4] Liu C, Fan YY, Liu M, Cong HT, Cheng HM, Dresselhaus MS. Hydrogen storage in single-walled carbon nanotubes at room temperature. Science 1999;286:1127-1129.

[5] Chen P, Wu X, Lin J, Tan KL. High H_2 uptake by Alkali-doped carbon nanotubes under ambient pressure and moderate temperatures. Science 1999;285:91-93.

[6] Yang RT. Hydrogen storage by alkali-doped carbon nanostructure-revisited. Carbon 2000;38:623-626.

[7] Atkinson K, Roth S, Hirscher M, Grünwald W. Carbon nanostructures: An efficient hydrogen storage medium for fuel cells?. Fuel Cells Bull 2001;38:9-12.

[8] Xu WC, Takahashi K, Matsuo Y, Hattori Y, Kumagai M, Ishiyama S, Kaneko K, Iijima S. Investigation of hydrogen storage capacity of various carbon materials. Int J of Hydrogen Energy 2007;32:2504-2512.

[9] Yang FH, Yang RT. Ab intio molecular orbital study of adsorption of atomic hydrogen on graphite: insight into hydrogen storage in carbon nanotubes. Carbon 2002;40:437-444.

[10] Anthony J, Lachawiec JR, Gongshin Qi, Yang RT. Hydrogen storage in nanostructured carbons by spillover: Bridge-building enhancement. Langmuir 2005;21:11418-11424.

[11] Li Y, Yang RT. Hydrogen storage in metal-organic frameworks by bridged hydrogen spillover. J Am Chem Soc 2006;128:8136-8137.

[12] Yildirim T, Ciraci S. Titanium-decorated carbon nanotubes as a potential high-capacity hydrogen storage medium. Phys Rev Lett 2005;94:175501-175504.

[13] Zhou L, Zhou Y. Determination of compressibility factor and fugacity coefficient of hydrogen in studies of adsorptive storage. Int J of Hydrogen Energy 2001;26:597–601.

[14] Mahanandia P, Vishwakarma PN, Nanda KK, Prasad V, Subramanyam SV, Dev SK, Satyam PV. Multiwall carbon nanotubes from pyrolysis of tetrahydrofuran. Mater Res Bull 2006;41:2311-2317.

[15] Rather SU, Zacharia R, Hwang SW, Naik MUD, Nahm KS. Hydrogen uptake of palladium-embedded MWCNTs produced by impregnation and condensed phase reduction method. Chem Phys Lett 2007;441:261-267.

[16] Zhao Y, Li CH, Yu ZX, Yao KF, Ji SF, Liang Ji. Effect of microstructures of Pt catalysts supported on carbon nanotubes (CNTs) and activated carbon (AC) for nitrobenzene hydrogenation. Mater Chem Phys 2007;103:225-229.

[17] Lewis FA. The hydrides of palladium and palladium alloys. Platinum Metals Rev. 1960;4(4):132-137.

[18] Yurum Y. Hydrogen energy system: production and utilization of hydrogen and future. Kluwer Academic Publishers, Dordrecht, 1995.

[19] Duś R, Nowicka E, Wolfram Z. Surface-Mediated formation of vanadium hydrides. Langmuir 1998;14:5487-5494.

[20] Yukawa H, Yamashita D, Ito S, Morinaga M, Yamaguchi S. Compositional dependence of hydriding properties of vanadium alloys at low hydrogen pressures. J Alloys and Compds 2003;356-357:45-49.

[21] Reilly JJ, Wiswall RH. BNL Report 16546. Brookhaven National Laboratory 1972.

[22] Yoo E, Gao L, Komatsu T, Yagai K, Yamazaki T, Matsuishi K, Matsumoto T, Nakamura J. Atomic hydrogen storage in carbon nanotubes promoted by metal catalysts. J Phys Chem B 2004;108:18903-18907.

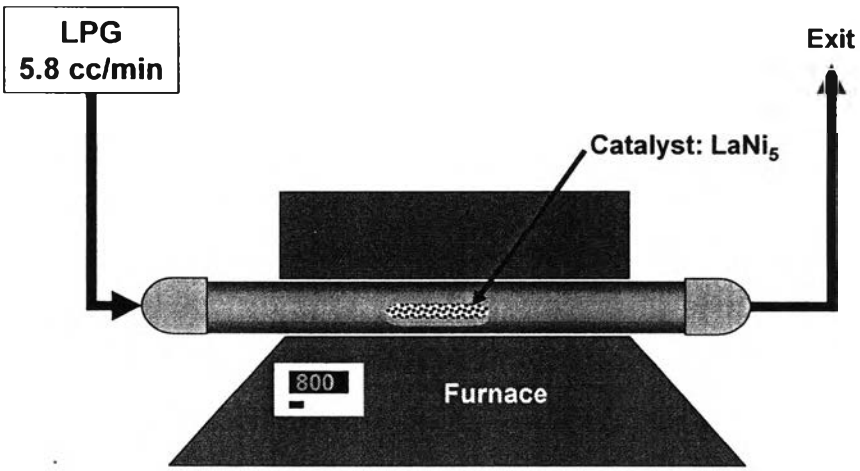

Figure 7.1 Schematic diagram of apparatus for CNT synthesis.

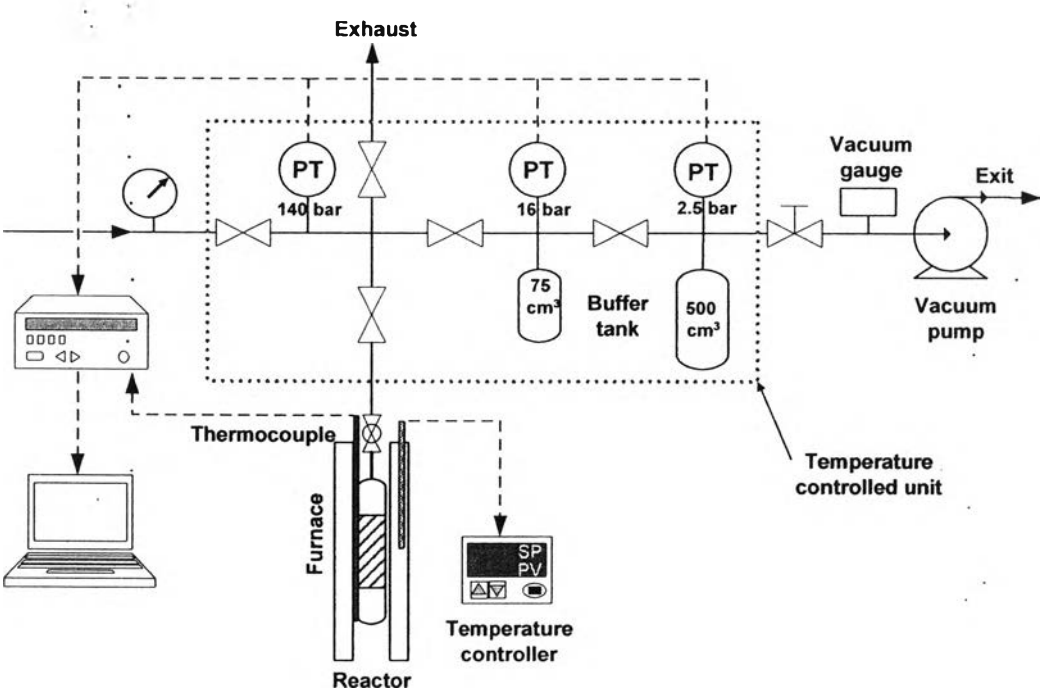

Figure 7.2 Schematic diagram of Seivert's apparatus.

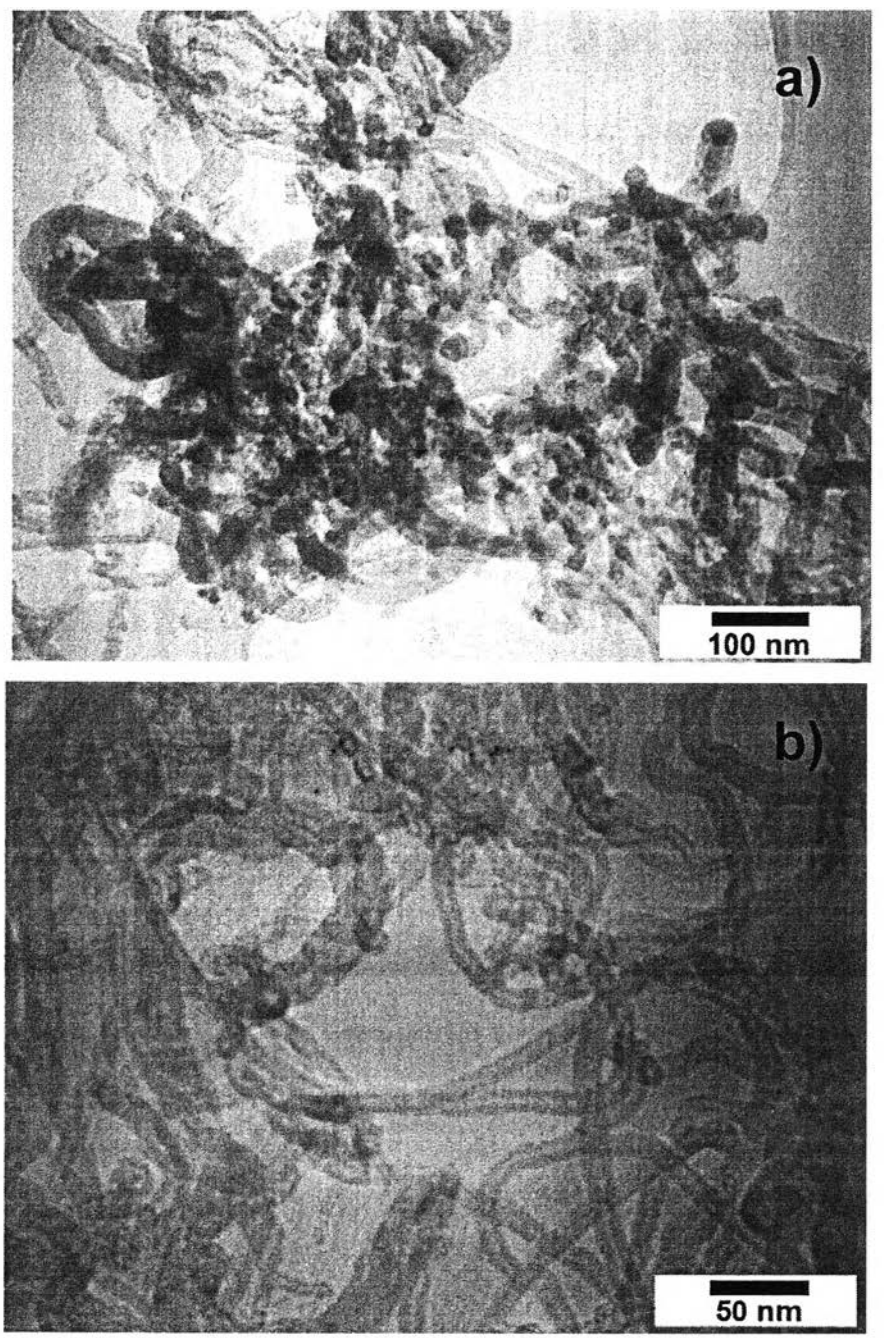

Figure 7.3 TEM images of CNTs a) raw CNTs and b) CNTs after treatment.

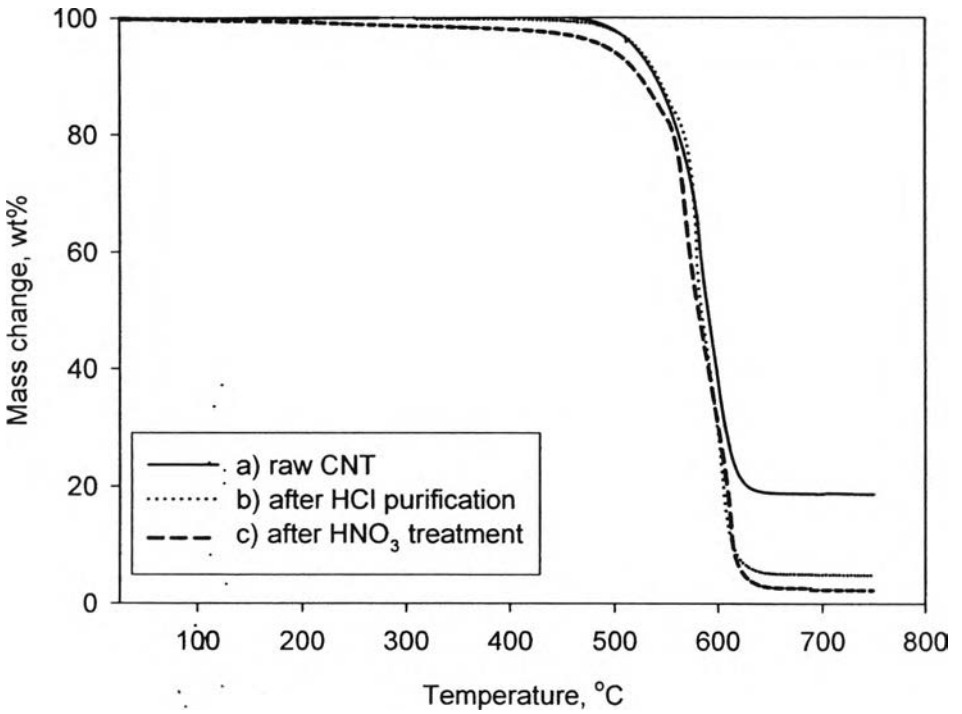

Figure 7.4 TGA analyses of CNTs a) raw CNTs, b) after HCl purification, and c) after HNO_3 treatment.

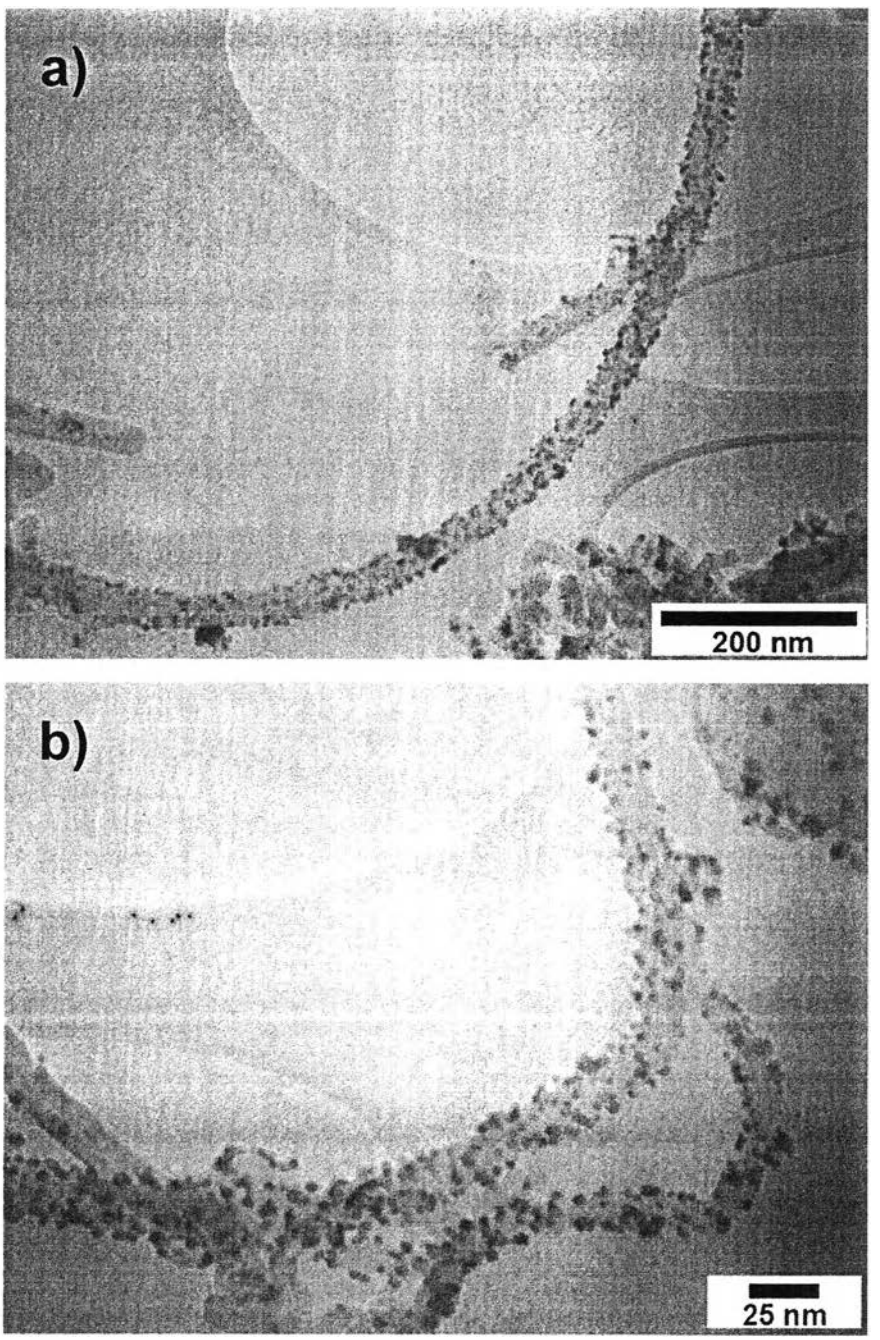

Figure 7.5 TEM images of Pd nanoparticles supported on CNTs a) at magnification of 100k and b) at magnification of 300k.

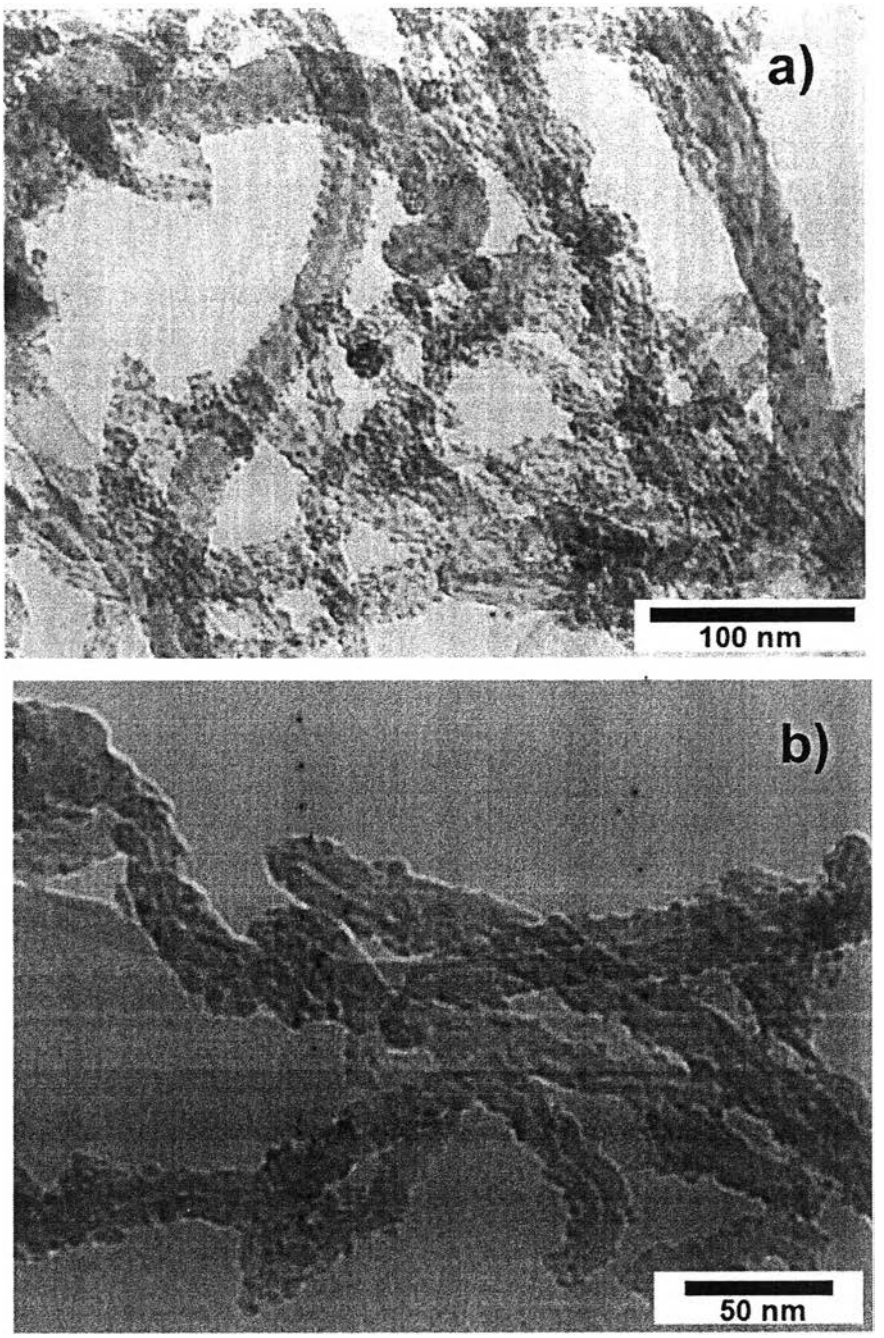

Figure 7.6 TEM images of V nanoparticles supported on CNTs a) at magnification of 200k and b) at magnification of 300k.

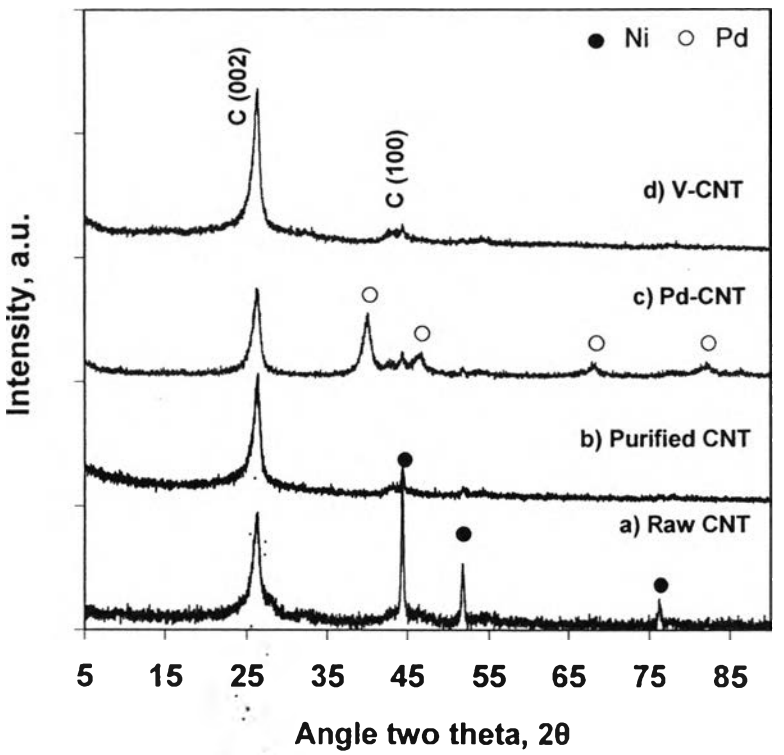

Figure 7.7 XRD patterns of a) raw CNTs, b) purified CNTs, c) Pd-CNTs, and d) V-CNTs.

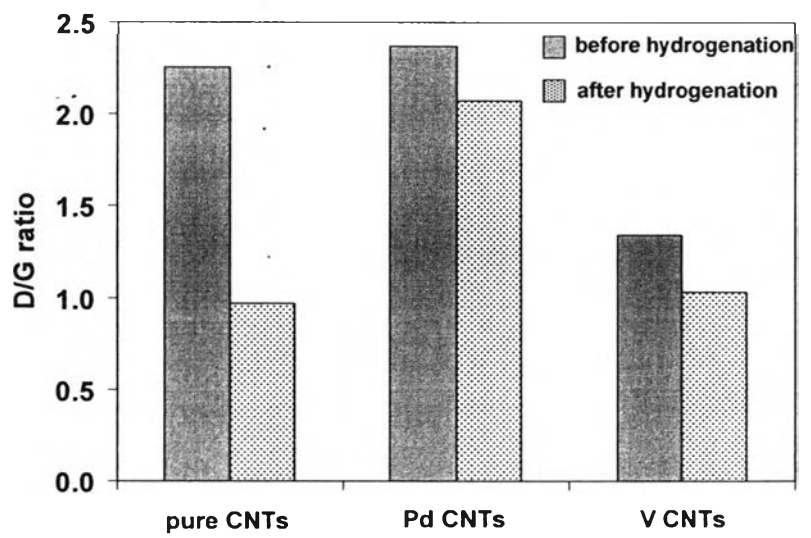

Figure 7.8 Area ratio of D and G band peaks for purified CNTs, Pd-CNTs, and V-CNTs.

Table 7.1 Specific surface area and hydrogen adsorption capacity of treated CNTs and deposited CNTs

Sample	*BET $m^2 g^{-1}$*	*metal content by ICP (wt%)*	*H_2 adsorption at -196°C (wt%)*	*H_2 adsorption at room temp. wt%*		*H_2 adsorption at room temp wt% (H/M)*	
				1^{st} ads	*2^{nd} ads*	*1^{st} ads*	*2^{nd}ads*
Treated CNTs	51.72 ± 0.04	-	1.21	<0.01	<0.03	-	-
Pd-CNTs	29.93 ± 0.07	7.91	0.37	0.125	0.065	1.556	0.815
V-CNTs	28.84 ± 0.12	5.28	0.40	0.10	0.08	1.859	1.493